Schwertmannite and Fe oxides formed by biological low-pH Fe(II) oxidation versus abiotic neutralization: Impact on trace metal sequestration

William D. Burgos [a,*], Thomas Borch [b,c], Lyndsay D. Troyer [c], Fubo Luan [a],
Lance N. Larson [a], Juliana F. Brown [a], Janna Lambson [d], Masayuki Shimizu [b]

[a] Department of Civil and Environmental Engineering, The Pennsylvania State University, University Park, PA 16802, United States
[b] Department of Chemistry, Colorado State University, Fort Collins, CO 80523-1872, United States
[c] Department of Soil and Crop Sciences, Colorado State University, Fort Collins, CO 80523-1170, United States
[d] Department of Biology, Washington University in St. Louis, St. Louis, MO 63105, United States

Abstract

Three low-pH coal mine drainage (CMD) sites in central Pennsylvania were studied to determine similarities in sediment composition, mineralogy, and morphology. Water from one site was used in discontinuous titration/neutralization experiments to produce Fe(III) minerals by abiotic oxidative hydrolysis for comparison with the field precipitates that were produced by biological low-pH Fe(II) oxidation. Even though the hydrology and concentration of dissolved metals of the CMD varied considerably between the three field sites, the mineralogy of the three iron mounds was very similar. Schwertmannite was the predominant mineral precipitated at low-pH (2.5–4.0) along with lesser amounts of goethite. Trace metals such as Zn, Ni and Co were only detected at μmol/g concentrations in the field sediments, and no metals (other than Fe) were removed from the CMD at any of the field sites. Metal cations were not lost from solution in the field because of unfavorable electrostatic attraction to the iron mound minerals. Ferrihydrite was the predominant mineral formed by abiotic neutralization (pH 4.4–8.4, 4 d aging) with lesser amounts of schwertmannite and goethite. In contrast to low-pH precipitation, substantial metal removal occurred in the neutralized CMD. Al was likely removed as hydrobasaluminite and $Al(OH)_3$, and as a co-precipitate into schwertmannite or ferrihydrite. Zn, Ni and Co were likely removed via adsorption onto and co-precipitation into the freshly formed Fe and Al solids. Mn was likely removed by co-precipitation and, at the highest final pH values, as a Mn oxide. Biological low-pH Fe(II) oxidation can be cost-effectively used to pretreat CMD and remove Fe and acidity prior to conventional neutralization techniques. A further benefit is that solids formed under these conditions may be of industrial value because they do not contain trace metal or metalloid contaminants.

© 2011 Elsevier Ltd. All rights reserved.

1. INTRODUCTION

Pennsylvania is currently the fourth largest coal producing state in the United States and has produced more than 25% of the total coal mined in the US during the past 200 years (USGS, 2008). These practices, though, have left their mark on the environment. Coal mine drainage (CMD) is a severe environmental threat to much of the Appalachian region of the US. Commonly referred to as acid mine drainage (AMD), CMD is marked by high concentrations of Fe and acidity. More than 10,000 km of streams in the Appalachian region are contaminated by AMD, with greater than 2000 km of those in Pennsylvania (Herlihy et al.,

1990). The cost of reclamation of contaminated watersheds in Pennsylvania alone is estimated between \$5 and \$15 billion (USGS, 2008).

Fe(III)-containing precipitates, often referred to as "yellowboy", are found at CMD sites coating rocks and streambeds. In certain settings where AMD springs emerge with elevated concentrations of Fe(II), biological low-pH Fe(II) oxidation produces terraced mounds of Fe(III) minerals that can be meters thick (DeSa et al., 2010). Most of these phases are amorphous; however, schwertmannite ($Fe_8O_8(OH)_x(SO_4)_y$; $x = 8 - 2y$, $1 < y < 1.75$), appears to be the predominant phase for low-pH water with high concentrations of sulfate while goethite can also be present in minor amounts (Bigham et al., 1990, 1996; Acero et al., 2006). Schwertmannite is metastable with respect to goethite and is often found on fresh depositional surfaces of AMD sites while goethite is found to increase with depth (Acero et al., 2006; Kumpulainen et al., 2007; Burton et al., 2008; Peretyazhko et al., 2009). The stability of schwertmannite can be enhanced by elevated concentrations of silica, phosphorus, and natural organic matter (Collins et al., 2010).

In order to offset the high costs associated with CMD treatment, it may be possible to collect the large amounts of Fe(III) precipitates at CMD sites for industrial reuse. Hedin et al. (1994) showed that Fe(III) precipitates formed at circumneutral pH and collected at CMD sites were similar to those mined for use as pigments. Since these pigments may be used in products such as cosmetics and ceramic serving ware, the incorporation of trace metals in the Fe(III) mineral is a potential concern. Due to kinetic limitations on abiotic Fe(II) oxidation at low pH, it is widely believed that acidophilic Fe(II)-oxidizing microorganisms are responsible for the majority of Fe(II) oxidation and subsequent precipitation of Fe(III) at AMD sites (Lane et al., 1992; Johnson et al., 2005; Senko et al., 2008). It is likely that the mineralogy and elemental composition of biogenic precipitates formed at low-pH CMD sites differ from those formed as a result of abiotic precipitation after neutralization of CMD.

There has been a great deal of research on the characterization of schwertmannite precipitation at low-pH and ferrihydrite precipitation at circumneutral-pH, as well as the conversion of schwertmannite to goethite (Bigham et al., 1996; Schwertmann and Carlson, 2005; Acero et al., 2006; Burton et al., 2008). However, little research has compared the incorporation of trace metal cations during low-pH biologically mediated precipitation to abiotic precipitation at higher pH. This is an important consideration for the remediation of heavy metal-laden AMD and industrial reuse of Fe(III) precipitates. The objectives of this study were to identify the mineral phases present and the extent of trace metal incorporation into precipitates formed in the field via low-pH Fe(II) oxidation at three AMD sites as compared to precipitates formed in the laboratory via abiotic neutralization at pH 4.38–8.35. The neutralization experiments were designed to mimic geochemical conditions encountered during alkali addition in a conventional AMD active treatment system.

2. MATERIALS AND METHODS

2.1. Site descriptions

Three CMD sites in western Pennsylvania were included in the current study: Lower Red Eyes in Somerset County, PA; Fridays-2 in Clearfield County, PA; and, Hughes Borehole in Cambria County, PA (Fig. 1). Physical characteristics and water chemistry for each site are provided in Table 1 and site schematics are provided in the Electronic Annex (Figs. EA-1–EA-3). Lower Red Eyes is a low flow (<1 L/s) CMD artesian spring that emerges within the Prince Gallitzin State Forest near Windber, PA (40° 14′ 25″ N; 78° 44′ 49″ W). The CMD is believed to originate from a nearby surface mine operated from the 1970s into the 2000s, and located along the Clarion, Brookville, and Kittanning coal seams. The CMD flows downstream across a spectacular series of iron terraces and pools (Fig. 1a) before eventually seeping back into the ground (150 m downstream of spring). This site is unique to the other two field sites in that the CMD is never hydrologically captured by a larger receiving stream, establishing a more extensive geochemical gradient. The CMD at this site is characterized by higher acidity, dissolved metals, and sulfate as compared to the other two field sites (Table 1).

Fridays-2 is the smaller of two CMD discharges (2.3 L/s) that drain the underground Fridays Mine complex. Fridays Mine is located in Hollywood, PA (41° 14′ 34″ N; 78° 32′ 28″ W) along the Kittanning coal seam and was first mined in the late 1800s (PA DEP, 2006). Fridays-2 emerges as an artesian spring at a collapsed mine entry, and flows 5–15 m over an iron mound before discharging to an unnamed tributary of Bennett Branch. The CMD flows over the mound as shallow (ca. 1 cm) sheet flow, and drops over a ca. 1 m tall terrace before immediately joining the tributary. The tall terrace contains unique stalactite-like Fe precipitates (Fig. 1d). Because of the higher flow rate and shorter path length across the iron mound, leading to a much shorter hydraulic residence time, the extent of Fe(II) oxidation at Fridays-2 is much less as compared to Lower Red Eyes (Table 1 and Fig. 2).

Hughes Borehole is a high flow (63 L/s) artesian spring that was purposefully drilled to drain a very large underground mine complex (2900 ha) near Portage, PA (40° 24′ 31″ N; 78° 39′ 17″ W) (DeSa et al., 2010). The CMD emerges near, and later flows into, the Little Conemaugh River. The CMD emergence is surrounded by a 0.61 ha iron mound that is up to 2 m deep. The CMD flows across the iron mound through relatively deep channels (ca. 0.6 m deep; captures most of the flow from the borehole) and as shallow sheet flow (ca. 1 cm deep) before discharging off the iron mound ca. 60 m downstream of the borehole.

2.2. Field sampling

Sampling locations were established as a function of distance downstream of each source along a single flow path that conveyed the majority of the water across each iron mound. Sediments were collected at different downstream distances to obtain solids that had formed under varying

Fig. 1. Field photographs of the AMD sites. Upstream view of pool and terraces at Lower Red Eyes (a). Upstream view of iron mound at Fridays-2 with large ledge in the bottom left corner (b). Downstream view of scoured channels on the iron mound at Hughes Borehole (c). Detail view of the large ledge at Fridays-2 where samples H1 and H4 were collected – note 50 mL tube (d).

geochemical conditions. Sediments were collected from areas of relatively fast and slow water velocities to obtain solids that been deposited under varying hydrological conditions. Sediments were collected from terraces, pools, and microterracettes to obtain solids from unique depositional *facies* (Fouke et al., 2000; Brown et al., 2010). Six to twelve sediment samples were collected from each site to capture any variances caused by these geochemical, hydrological, and geomorphological differences. Sediments were collected from the top 2 cm of the iron mounds, transported on ice, and stored under atmospheric conditions at 4 °C until analysis.

Two core samples (designated as H1 and H4) were collected horizontally into the vertical face of the tall terrace (ca. 6 cm penetration depth) that marked one edge of the iron mound at Fridays-2 (Fig. 1b and d). Photographs of the collected sediment cores are included in the Electronic Annex (Fig. EA-4). Location H1 was collected from the terrace directly below the primary flowpath from the borehole, while H4 was collected from the terrace ca. 1 m to the right/downhill of H1. The soil cores were plugged with rubber stoppers and immediately stored in an airtight, N_2-flushed ammunition box, and then kept at 4 °C. The box was opened in an anaerobic chamber (95:5% N_2:H_2) and the soil cores were divided into three sections, each approximately 2 cm long, and dried in the chamber prior to analysis.

Dissolved oxygen (DO) was measured using an Oakton DO 300 Series field meter; temperature, pH, and oxidation–reduction potential (ORP) were measured with Beckman Φ265 pH/Temp/mV meters; and conductivity was measured using an Oakton CON 400 series field meter. Filtered (0.45 μm) water samples were preserved in the field with HCl (for dissolved Fe(II) analysis) or HNO_3 (for dissolved

metals analysis by inductively coupled plasma-atomic emission spectroscopy, ICP-AES). Samples for sulfate analysis were neither filtered nor acidified. All water samples were transported on ice and stored at 4 °C until analysis.

2.3. Laboratory abiotic neutralization experiments

Water was collected from the emergent Lower Red Eyes spring by completely submerging 10 L high density polyethylene (HDPE) plastic containers ca. 10 cm below the water surface. DO was below detection (<0.5 μM), pH was 4, and ORP was 225 mV at both times of collection (July 2009, October 2010). Containers were filled underwater with no headspace, capped underwater, and then stored on ice during transport. The water was then filtered (0.45 μm) and stored in another plastic container with no headspace at 4 °C. No attempt was made to maintain anoxic conditions after filtration.

The filtered Lower Red Eyes water was used in discontinuous titration/neutralization experiments to produce Fe(III) precipitates via abiotic reactions at a number of elevated pH values. The theoretical total acidity of the Lower Red Eyes water was calculated based on pH and measured concentrations of dissolved Fe(II), Fe(III), Mn, and Al according to Kirby and Cravotta (2005), and found to equal 28.3 meq/L. Four acid-washed HDPE plastic bottles were filled with 250 mL of Lower Red Eyes water. NaOH was titrated into Lower Red Eyes water in aliquots equivalent to ¼ of the theoretical total acidity of the water, until the pH of the system reached pH 8.3. This amounted to first adding 17.8 mL of 0.10 N NaOH to each bottle of Lower Red Eyes water (i.e., to complete 25% of the neutralization). The bottles were stirred to maintain a small vortex

Table 1
Water chemistry of the emergent springs at Lower Red Eyes, Fridays-2, and Hughes Borehole.

	Lower Red Eyes	Fridays-2	Hughes Borehole
Flow (L/s)	0.4	2.3	20–125
Temp. (°C)	9.4 ± 0.7	9.8 ± 0.1	12.7 ± 0.6
	$N = 7$	$N = 4$	$N = 30$
DO (μM)	<0.5	11.3 ± 13.4	34.4 ± 25.0
	$N = 2$	$N = 4$	$N = 21$
Conductivity (mS/cm)	4.36 ± 0.16	0.772 ± 0.001	1.08 ± 0.1
	$N = 7$	$N = 2$	$N = 23$
pH	4.04 ± 0.25	4.1 ± 0.2	3.96 ± 0.25
	$N = 7$	$N = 4$	$N = 29$
Dissolved total Fe[a] (μM)	9620 ± 387	865 ± 105	1590 ± 6
	$N = 5$	$N = 4$	$N = 7$
Dissolved Fe(II)[a] (μM)	9720 ± 326	840 ± 108	1790 ± 312
	$N = 5$	$N = 5$	$N = 25$
Al (μM)	1590 ± 43	741 ± 89	304 ± 14
	$N = 3$	$N = 6$	$N = 7$
Mn (μM)	2060 ± 53	24 ± 2	44 ± 0.4
	$N = 3$	$N = 6$	$N = 7$
Co (μM)	2060 ± 53	n.a.	3.22 ± 0.17
	$N = 3$		$N = 7$
Ni (μM)	138 ± 83	n.a.	6.82 ± 0.17
	$N = 3$		$N = 7$
Zn (μM)	199 ± 23	n.a.	4.13 ± 0.15
	$N = 3$		$N = 7$
As (μM)	<0.67	n.a.	<0.13
	$N = 3$		$N = 7$
SO_4^{2-} (μM)	$31{,}170 \pm 3833$	3410 ± 770	5970 ± 660
	$N = 12$	$N = 4$	$N = 5$
Acidity(mM $CaCO_3$/L)	14.2 ± 0.05	2.07 ± 0.05	2.3 ± 0.05
	$N = 2$	$N = 4$	$N = 7$
Si (μM)	423 ± 5.1	792 ± 143	630 ± 8.5
	$N = 2$	$N = 4$	$N = 7$
TOC (μM)	91.7	167 ± 100	72.5 ± 18
		$N = 3$	$N = 3$
PO_4^{3-} (μM)	5.3 ± 0.7	n.a.	6.2 ± 3.2
	$N = 3$		$N = 3$

[a] Dissolved total Fe measured by ICP-AES, dissolved total Fe(II) measured by ferrozine.

and purged continuously with compressed air for 1 h, and then refrigerated overnight. The following day, the bottles were removed from the refrigerator to come to room temperature, the pH was measured in the overlying water in all four bottles, and one bottle was returned to the refrigerator (pH 5.18). For the remaining three bottles, another 17.8 mL of 0.10 N NaOH was added to each bottle and identical procedures were followed over the next three days to produce suspensions equivalent to 50 (pH 5.36), 75 (pH 6.21), and 100% neutralization (pH 8.34). One day after the 100% neutralization suspension was produced; all of the suspensions were transferred to centrifuge tubes and centrifuged at 8000 rpm for 10 min. Supernatant samples were collected and preserved with HNO_3 for dissolved metals analysis by ICP-AES, and concentrations were calculated to account for sample dilution with NaOH. Pelletized precipitates were rinsed once with distilled–deionized water, and air-dried for SEM analysis or dried under nitrogen for XRD analysis.

This experiment was repeated with the October 2010 water to generate solids for Fe K-edge EXAFS analysis. During this repeat experiment pH and ORP were monitored continuously over the four days allowed for precipitates to form. ORP was measured after calibrating with a freshly prepared +228 mV Zobel standard solution. Suspensions were mixed and bubbled with air continuously, and maintained at room temperature (22–25 °C) over the four days. For suspensions with NaOH added equivalent to 25%, 50%, 75% and 100% neutralization, final pH values were 4.38, 4.40, 7.03 and 8.35, respectively. An additional sample was prepared where NaOH was added equivalent to 100% neutralization in one single aliquot (71.2 mL 0.1 N NaOH to 250 mL of Lower Red Eyes water). The final pH for this suspension was 8.13. Supernatant and solid samples were prepared as described above.

2.4. Analytical methods

Dissolved metal concentrations were analyzed on a Perkin-Elmer Optima 5300 ICP-AES. Dissolved Fe(II) concentrations were measured by ferrozine. Field sediments and laboratory precipitates were sieved (<1-mm) and ground into fine powders. The composition of metal oxides was determined for field sediments via ICP-AES, after lithium
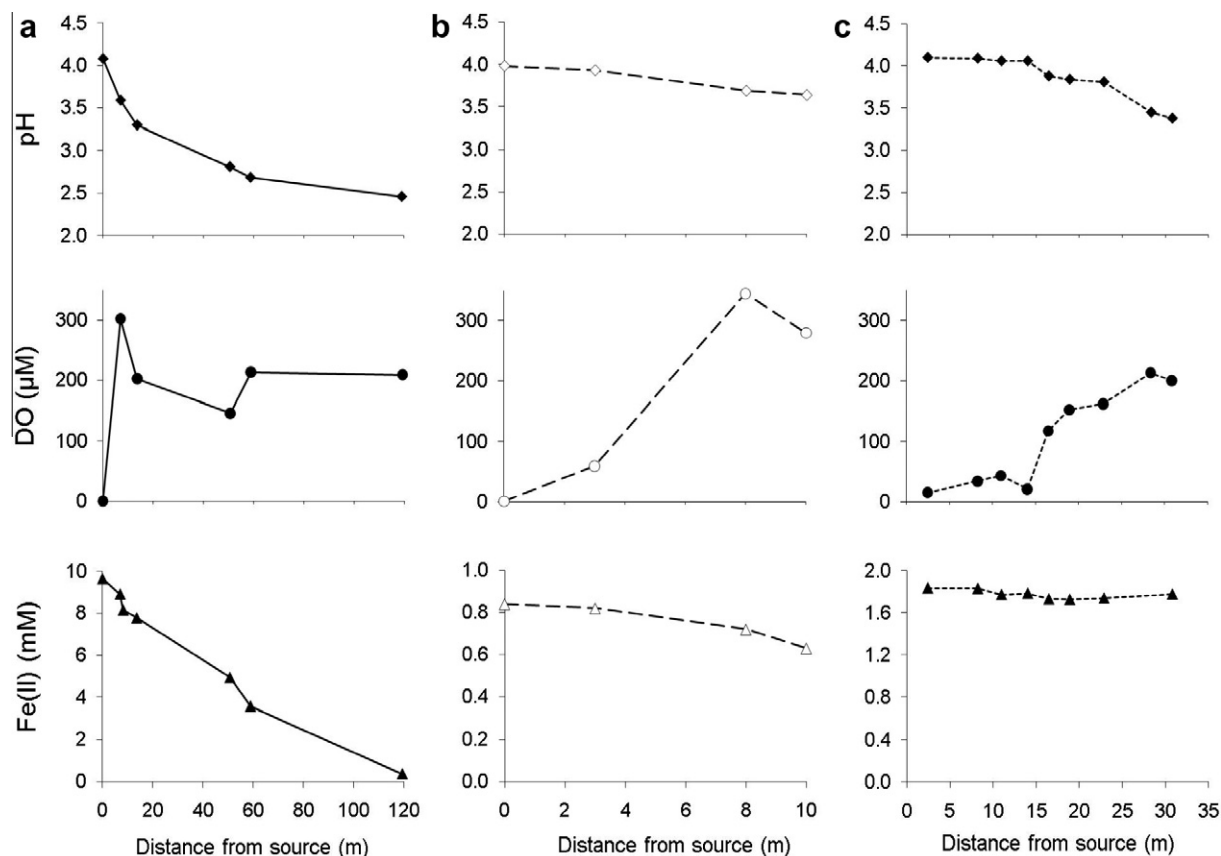
Fig. 2. Water chemistry trends for Lower Red Eyes (July 2009) (a), Fridays-2 (July 2006) (b), and Hughes Borehole (August 2007) (c).

metaborate fusion at 1000 °C. Laboratory precipitates produced from Lower Red Eyes water and field samples collected from the Lower Red Eyes iron mound were dissolved in ammonium oxalate (28 g/L ammonium oxalate + 15 g/L oxalic acid, pH ~2.7) and 6 N HCl, respectively, to operationally distinguish poorly crystalline iron oxides (schwertmannite and ferrihydrite) from less soluble crystalline iron oxides (goethite) (Peretyazhko et al., 2009). Fifty mg dried solids were reacted with 50 mL of each reagent for 1 h, then centrifuged and supernatant samples were preserved with HNO_3 prior to analysis by ICP-AES.

Sediment samples were prepared for scanning electron microscopy (SEM) following procedures described by Zhang et al. (2007). Samples were preserved in the field with 2.5% glutaraldehyde and prepared for imaging with a series of ethanol dehydrations followed by critical point drying. Dried samples were mounted onto carbon SEM stubs and imaged on an FEI Quanta 200 environmental SEM under low vacuum. Higher magnification images were collected using a Jeol JSM-6700F field emission SEM with a working distance of 3 mm.

Powder X-ray diffraction patterns were collected using a Rigaku D/Max Rapid II X-ray diffractometer (XRD) with a Mo X-ray tube and a 0.3 mm collimator. Intensities were measured with the omega axis fixed at 0° and phi axis oscillation between −20° and +20° with a 10 min exposure time. Data was integrated from 0° to 360° with a step size of 0.02

using AreaMax software and all data analysis was performed using Jade 7 software.

Dry samples for X-ray absorption spectroscopic analyses were diluted with boron nitride and packed in Teflon sample holders and sealed with a Kapton polyimide film to prevent oxidation while minimizing X-ray absorption. The structural environment of Fe was determined using extended X-ray absorption fine structure (EXAFS) spectroscopy at the Stanford Synchrotron Radiation Lightsource (SSRL). Data were collected for the Fridays-2 samples on beamline 10-2 (26-pole wiggler). The storage ring was operated at 3.0 GeV and at currents between 60 and 100 mA. Data for the abiotic precipitation samples were collected on beamline 4-3 (20-pole wiggler). The storage ring was operated at 3.0 GeV at a current of 300 mA. The Fe EXAFS analytical procedures used here were similar to those described previously (Borch et al., 2006; Jacquat et al., 2009; Moberly et al., 2009). Energy selection was accomplished with a Si (111) monochromator and spectra were recorded in X-ray transmission mode using ion chambers. A set of Fe reference compounds was used to perform linear combination (LC) k^3-weighted EXAFS spectral fitting using the SIXPACK interface to IFEFFIT (Webb, 2005). Principal component analysis was performed on sample spectra to estimate the number of reference compounds required for LC fitting. Fe EXAFS reference spectra for ferrihydrite, schwertmannite and goethite are included in the Electronic Annex (Fig. EA-5). The appropriate Fe reference

spectra were identified using target transformation (TT) testing. Based on the SPOIL value from TT testing, preliminary LC fitting, appearance in XRD patterns, and their likelihood of formation based on reaction path modeling; schwertmannite, goethite and ferrihydrite were specifically selected as reference compounds. The SPOIL values for schwertmannite and ferrihydrite were greatly different from each other, which implies that these reference spectra are different from each other (Fig. EA-5). Reference compounds were included in the fit only if they contributed more than 5% mol/mol, equivalent to our detection limit for minor constituents (Hansel et al., 2003). Linear combinations of the reference compounds were optimized and the only variable parameters were the mole fractions of each reference compound.

3. RESULTS

3.1. AMD chemistry

The three field sites we studied all contained iron mounds that formed via biological low-pH Fe(II) oxidation (Fig. 1), while the water chemistry (Table 1), geochemical gradients (Fig. 2), and hydrodynamics across the iron mounds varied considerably. The importance of biological Fe(II) oxidation was confirmed through a series of laboratory experiments using live and sterilized sediments from Lower Red Eyes (Brown et al., 2010), Fridays-2 (Lucas, 2008) and Hughes Borehole (DeSa et al., 2010). Lower Red Eyes had the highest concentrations of metals, acidity, and sulfate, the lowest flow rate, and the longest residence time across its iron mound (Table 1). The influx and saturation of DO, and decreases in pH, dissolved Fe(II) and dissolved Fe are consistent with biologically-mediated low-pH Fe(II) oxidation and Fe(III) hydrolysis and precipitation (Fig. 2a). Fridays-2 had the lowest concentration of Fe(II), acidity, and sulfate, an intermediate flow rate, and likely the shortest residence time across its iron terrace. Hughes Borehole had intermediate concentrations of Fe(II), acidity, and sulfate, an extremely high flow rate, and variable residence times across its iron mound because of a combination of flow along scoured channels or across shallow microterracettes. Even though dissolved Fe(II) and dissolved total Fe concentrations did not drop dramatically across the Hughes Borehole iron mound (Fig. 2c), Fe precipitation over the past several decades has produced mound sediments 1–2 m deep.
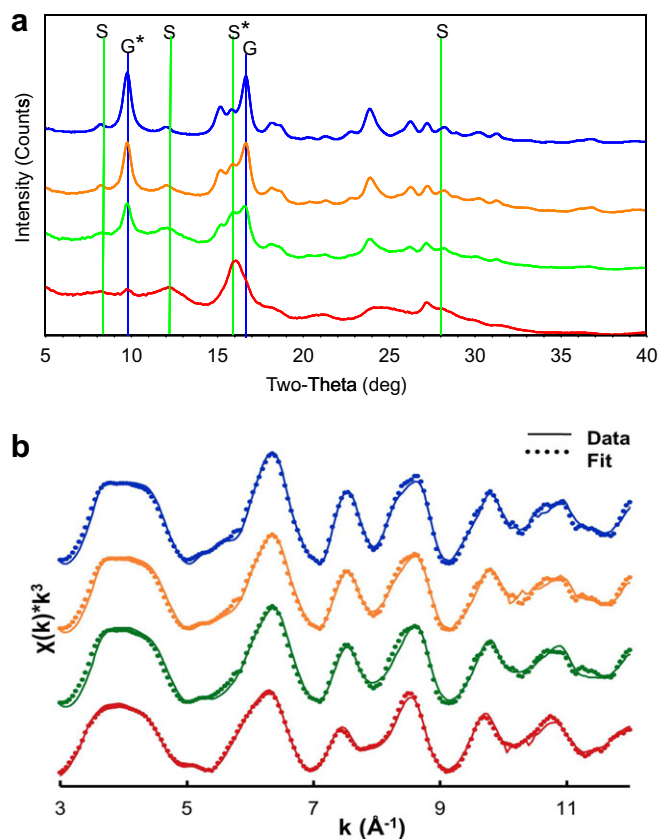

Fig. 3. X-ray diffraction patterns (a) and Fe K-edge EXAFS spectra (b) from field samples collected from Fridays-2. Samples were collected 10 m downstream of emergent AMD spring from the vertical face of a large ledge. Core samples (6 cm penetration depth) were collected horizontally into the ledge face at two locations, H1 and H4. H1 was directly below the primary flowpath while H4 was 1 m to the right/ downhill of H1. Patterns are arranged top to bottom, respectively, for samples with highest to lowest goethite contents and are in identical order in (a) and (b). Top pattern from H1 0–2 cm depth, 2nd pattern from H1 4–6 cm depth, 3rd pattern from H4 0–2 cm depth, and bottom pattern from H4 4–6 cm depth. In (a) G = goethite, S = schwertmannite, and ∗ designates peak with greatest intensity in reference pattern. Details for fits of the Fe K-edge EXAFS spectra in (b) are provided in Table 2.

3.2. Mineralogy of natural sediments produced via biological low-pH Fe(II) oxidation

Iron precipitates varied across these sites with respect to their physical features and morphology. For example, at Lower Red Eyes, the iron mound was classified into unique depositional *facies* such as terraces, pools, and microterracettes (Fouke et al., 2000; Brown et al., 2010). Terraces consisted of vertical drops greater than 5 cm, pools with diameters of 1–2 m contained quiescent water, and microterracettes consisted of vertical drops less than 2 cm. At Fridays-2, the predominant depositional *facie* was microterracettes, but there was one tall terrace (1 m) that the CMD ran over before entering the adjacent unnamed tributary. At Hughes Borehole, the predominant depositional *facie* was microterracettes, however, the majority of the CMD was conveyed along deep (0.5 m), narrow (1 m wide) scoured channels. We found that schwertmannite was the predominant mineral across these iron mounds while goethite was found in smaller amounts (Figs. 3 and 4).

Based on comparisons of XRD patterns and LC fitting of Fe K-edge EXAFS spectra (Fig. 3 and Table 2), we qualitatively ranked the goethite content of all of the sediments based on the XRD peak intensity at 9.73° two theta. From this we then arranged all of the XRD patterns from each site (6–12) in order of highest to lowest goethite content. In Figs. 3a and 4 we selected four patterns from each site that captured the whole range of schwertmannite-to-goethite ratios observed for each site. We found that there were no observable systematic trends in iron mineralogy with respect to location on the iron mound (i.e., along a geochemical gradient), or with respect to the sample location's water velocity (i.e., across a hydrodynamic gradient), or with respect to the depositional *facies* where the sediments were formed. No mineralogical phases other than schwertmannite and goethite were detected at any field site. SEM analysis of all field samples also revealed a predominance of spherical particles (1–2 μm diameter) with a "hedgehog" morphology characteristic of schwertmannite (Fig. 5a–d). The average Fe/S molar ratio in the Lower Red Eyes sediments was 5.42 ± 0.83 ($n = 4$) (based on HCl digestions, Table 3), corresponding to a schwertmannite stoichiometry of $Fe_8O_8(OH)_5(SO_4)_{1.5}$ (with reported values of $1 < SO_4 < 1.75$).

Based on LC fitting of Fe K-edge EXAFS spectra, goethite decreased with horizontal distance into the tall terrace at Fridays-2 (Fig. 3b and Table 2). The surface section of sample H1 (0–2 cm horizontal penetration into the vertical
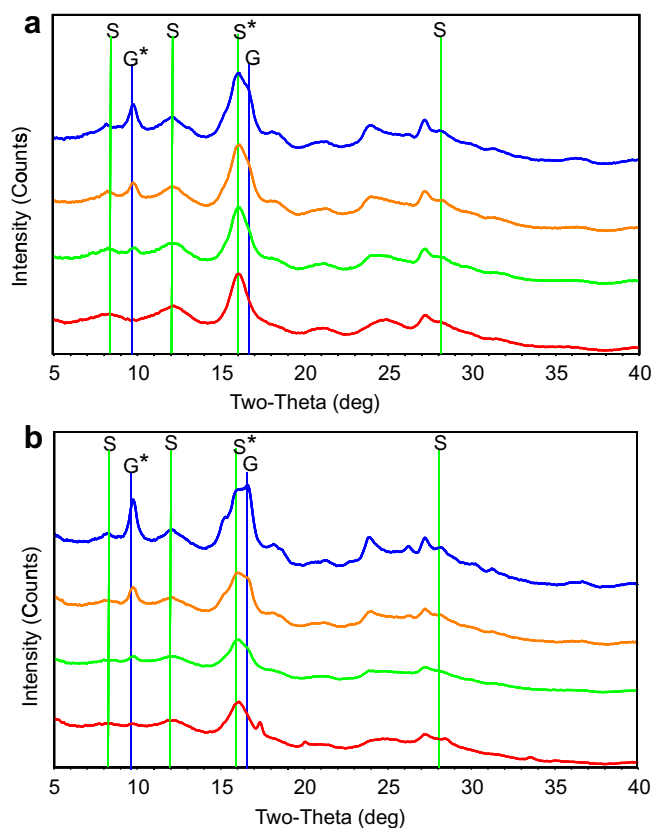

Fig. 4. X-ray diffraction patterns from samples collected from Lower Red Eyes (a) and Hughes Borehole (b). In both panels, patterns are arranged top to bottom, respectively, for samples with highest to lowest goethite contents. (a) Top pattern from pool *facies* 59 m downstream of Lower Red Eyes spring, 2nd pattern from terrace 62 m downstream, 3rd pattern from terrace 52 m downstream, and bottom pattern from pool 14 m downstream. (b) Top pattern from the main scoured channel 8 m downstream of Hughes Borehole, 2nd pattern from terrace *facies* 60 m downstream, 3rd pattern from microterracette 31 m downstream, and bottom pattern from pool 55 m downstream. G = goethite, S = schwertmannite, and ∗ designates peak with greatest intensity in reference pattern.

Table 2
Mineralogical composition of samples based on linear combination fitting of Fe K-edge EXAFS spectra. Field samples were collected from Fridays-2 (H1, H4) and solids were formed in the laboratory via abiotic neutralization/precipitation from Lower Red Eyes water. Precision of fits is ca. 5 mol%.

Sample	Schwertmannite mol% Fe	Goethite mol% Fe	Ferrihydrite mol% Fe	Red. χ^2
H1 0–2 cm depth	44.6	55.4	–	0.08
H1 4–6 cm depth	55.7	44.3	–	0.08
H4 0–2 cm depth	58.9	41.1	–	0.11
H4 4–6 cm depth	68.3	31.7	–	0.17
Abiotic precipitate pH 4.38	38.1	16.8	45.1	0.19
Abiotic precipitate pH 4.40	33.2	17.1	49.7	0.11
Abiotic precipitate pH 7.03	30.2	10.0	59.8	0.10
Abiotic precipitate pH 8.13	20.5	10.1	69.4	0.16
Abiotic precipitate pH 8.35	21.9	7.0	71.1	0.11

terrace face) consisted of 45% schwertmannite, 55% goethite, while the deeper section (4–6 cm horizontal penetration) consisted of 56% schwertmannite and 44% goethite (all estimates ±5%). A similar difference along the horizontal penetration depth into the terrace was found in sample H4. The first 0–2 cm into the ledge was composed of 59% schwertmannite and 41% goethite, while the sample 4–6 cm into the ledge was composed of 68% schwertmannite and 32% goethite. Because schwertmannite is metastable with respect to goethite, sample locations with high schwertmannite-to-goethite ratios should reflect conditions that stabilize schwertmannite. The Lower Red Eyes AMD contained the highest sulfate concentration which should favor the stabilization of schwertmannite, while the Fridays-2 AMD contained the lowest sulfate concentration which could favor the conversion of schwertmannite to goethite. In addition to sulfate, silica, phosphorus and dissolved organic carbon (DOC) have been shown to stabilize schwertmannite with respect to Fe(II)-catalyzed conversion to goethite (Jones et al., 2009). At these three sites, dissolved Si concentrations ranged from 420 to 790 μM, dissolved phosphate concentrations were around 5–6 μM (but less downstream of the springs), and DOC concentrations ranged from 70 to 170 μM (Table 1). Jones et al. (2009) showed that 1 mM dissolved Si completely stabilized schwertmannite while 25 mg/L Suwannee River fulvic acid (equivalent to ca. 1 mM DOC) partially stabilized schwertmannite. We speculate that Si concentrations below 1 mM, rather than P or DOC, stabilized schwertmannite at our field sites.

3.3. Mineralogy from abiotic precipitation experiments

Discontinuous titration/neutralization experiments were conducted with Lower Red Eyes water to produce solids that formed at elevated pH values (pH 4.4–8.4) as compared to field conditions (emergent pH 4.0 declined to pH 2.5; Fig. 1a). Our motivation for conducting these experiments was to examine trace metal partitioning under relatively high pH conditions encountered in AMD active treatment systems as compared to natural low-pH iron mound sediments. We conducted these experiments on two different occasions with water collected in July 2009 and October 2010, however, the water chemistry of the emergent Lower Red Eyes spring was essentially identical. In our first experiment, the discontinuous titration process

yielded precipitates that formed at final pH values of 5.18, 5.36, 6.21, and 8.34. After the first aliquot of NaOH was added (day 0), an orange precipitate formed and its color remained unchanged for the whole 4 d reaction period (final pH 5.18). After the second aliquot of NaOH was added (day 1), a dark green precipitate formed initially but then became orange after 1 h (final pH 5.36). After the third aliquot of NaOH was added (day 2) a green precipitate formed initially but then became orange-brown (final pH 6.21). After the fourth and final aliquot of NaOH was added (day 3), an orange precipitate formed and its color remained unchanged for the remainder of the reaction period (final pH 8.34).

During our second experiment we continuously monitored the pH and ORP of the suspensions during the whole 4 d reaction period (Fig. 6). In this repeat experiment, the discontinuous titration process yielded precipitates that formed at final pH values of 4.38, 4.40, 7.03, and 8.35. In contrast to the first experiment where we mixed and aerated the suspensions for 1 h after NaOH addition and then stored the suspension at 4 °C until the next day, in this repeat experiment we continuously mixed and aerated the suspensions so that we could continuously monitor pH and ORP. Continuous aeration promoted greater Fe(II) oxidation in the first two suspensions (i.e., one and two additions of NaOH), and the subsequent precipitation of more Fe(III) decreased the final pH values to 4.38 and 4.40 (as compared to final pH values of 5.18 and 5.36 in the first experiment). Continuous monitoring of pH and ORP in these suspensions clearly showed that the geochemical conditions varied much more than just the differences between the initial and final conditions. For example, while we designated the first suspension as "abiotic precipitate pH 4.38", over its 4 d reaction period the suspension pH varied from pH 3.72 to 5.89 and the ORP varied from –9 to +300 mV (Fig. 6a). In the first 10 min (inset in Fig. 6a), the pH increased quickly because of the instantaneous dosing of NaOH while the ORP decreased because the initial oxidation rate of Fe(II) exceeded the mass transfer rate of O_2. The subsequent decrease in pH was caused by hydrolysis of the Fe(III) that had been produced while the subsequent increase in ORP demonstrated that the mass transfer rate of O_2 began to exceed the oxidation rate of Fe(II). Similarly, for the suspension that was discontinuously dosed with four aliquots of NaOH and designated
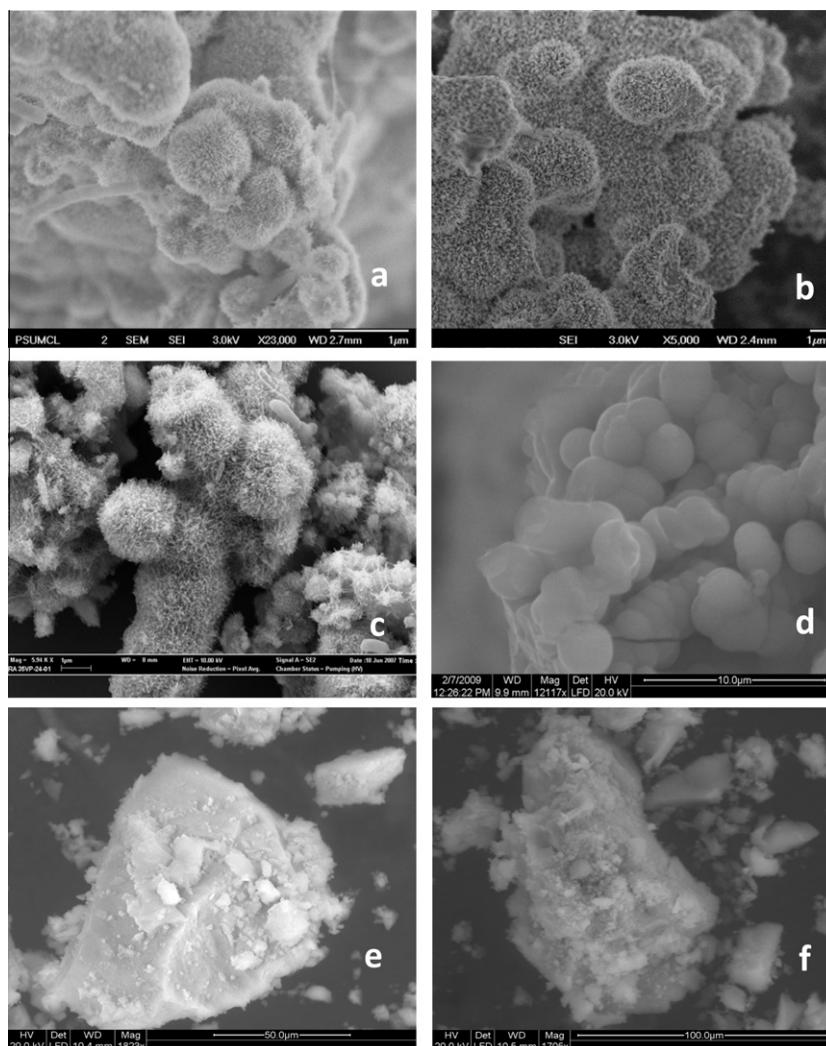
Fig. 5. SEM images of representative samples from: Lower Red Eyes at the AMD source (a); Lower Red Eyes at a downstream pool (b); Fridays-2 (c); Hughes Borehole (d); and solids formed in the lab from Lower Red Eyes water via abiotic neutralization/precipitation at final pH 4.38 (e) and final pH 8.13 (f).

as "abiotic precipitate pH 8.35", over its 4 d reaction period the suspension pH varied from pH 3.72 to 9.38 while its ORP varied from –100 to +300 mV (Fig. 6b). These large changes in pH and pe (i.e., ORP) span mineral stability fields of schwertmannite, goethite and ferrihydrite. In other words, all of these minerals could have potentially formed as the water chemistry evolved over the different reaction periods (e.g., as reaction path "trajectories" plotted on a pe-pH diagrams; Figs. EA-6 and EA-7 in the Electronic Annex; generated using Geochemists Workbench and the water chemistry of Lower Red Eyes in Table 1).

Based on XRD patterns (Fig. 7a) and LC fitting of the Fe K-edge EXAFS spectra (Fig. 7b and Table 2), a combination of schwertmannite, goethite, and ferrihydrite were identified in all of the precipitates formed via abiotic neutralization. We found that abiotic precipitates formed at pH 4.38 contained 38% schwertmannite, 17% goethite, and 45% ferrihydrite, similar to LC fitting results for the solids formed at pH 4.40. As the final pH of the abiotic pre-

cipitates increased, the mole fractions of schwertmannite and goethite decreased while the fraction of ferrihydrite increased. Abiotic precipitates formed at pH 8.35 contained 22% schwertmannite, 7% goethite, and 71% ferrihydrite. SEM analysis of the neutralized precipitates revealed distinctly different particle morphologies (Fig. 5e and f) as compared to field samples (Fig. 5a–d). Instead of spheres with a hedgehog texture, neutralized precipitates appeared as laths fused into much larger particles. Characteristic dimensions of these laths were difficult to generalize from these SEM micrographs. This altered morphology was similar to observations reported by Acero et al. (2006) coincident with schwertmannite transformation into goethite in aging experiments (353 d) where the pH decreased from pH 3.07 to 1.74.

Higher amounts of schwertmannite at pH 4.38 and 4.40 were consistent with higher solid-phase S/Fe ratios measured in these precipitates as compared to precipitates formed at pH > 7 (Table 3). It is important to note that

ARTICLE IN PRESS

Table 3
Metal content of solids formed via abiotic neutralization/precipitation in the laboratory, and for sediments collected from Lower Red Eyes and Hughes Borehole. Solids were dissolved in 6 N HCl and ammonium oxalate.

Sample ID	Fe_{HCl} (mmol/g)	Fe_{ox} (mmol/g)	S_{HCl} (mmol/g)	S_{ox} (mmol/g)	Al_{HCl} (µmol/g)	Al_{ox} (µmol/g)	Mn_{HCl} (µmol/g)	Mn_{ox} (µmol/g)	Co_{HCl} (µmol/g)	Co_{ox} (µmol/g)	Ni_{HCl} (µmol/g)	Ni_{ox} (µmol/g)	Si_{HCl} (µmol/g)	Si_{ox} (µmol/g)	Zn_{HCl} (µmol/g)	Zn_{ox} (µmol/g)
Abiotic precipitate pH 4.38	6.06	4.19	1.73	1.23	3380	2380	3	1.6	5	3.7	14	11	159	81	30	22
Abiotic precipitate pH 4.40	6.15	5.12	1.01	0.96	1380	1200	2	1.9	3	3.0	13	11	114	75	34	30
Abiotic precipitate pH 7.03	6.80	6.36	0.57	0.53	1180	1080	141	140	37	36	61	59	288	260	150	144
Abiotic precipitate pH 8.13	5.55	5.58	0.37	0.35	950	930	1160	1150	42	42	55	56	255	235	124	125
Abiotic precipitate pH 8.35	5.76	5.22	0.33	0.35	1010	990	1260	1250	44	44	59	59	269	233	132	127
Lower Red Eyes upper pool[a]	7.89	0.42	1.72	0.03	29	2.6	2.3	0.4	1.9	0.00	0.78	0.10	41.8	2.0	0.95	3.8
Lower Red Eyes upper terrace[a]	8.55	1.27	1.78	0.41	22	2.7	2.3	1.1	2.3	0.03	1.2	0.12	46.7	5.0	2.1	0.8
Lower Red Eyes lower pool[a]	7.43	0.73	1.22	0.26	14	3.9	1.9	1.1	0.21	0.02	0.16	0.12	26.7	4.2	1.2	0.8
Lower Red Eyes lower terrace[a]	8.56	1.15	1.39	0.42	10	1.5	1.8	1.1	2.4	0.04	2.2	0.12	50.8	4.1	3.5	1.4

[a] Lower Red Eyes sediment sampling locations refer to depositional *facies* where samples were collected. Upper terrace and pool sediments were collected 27 m downstream from the emergent AMD spring, lower terrace and pool sediments were collected 60 m downstream, emergent pool was collected 0 m downstream, and top terrace was collected 11 m downstream.
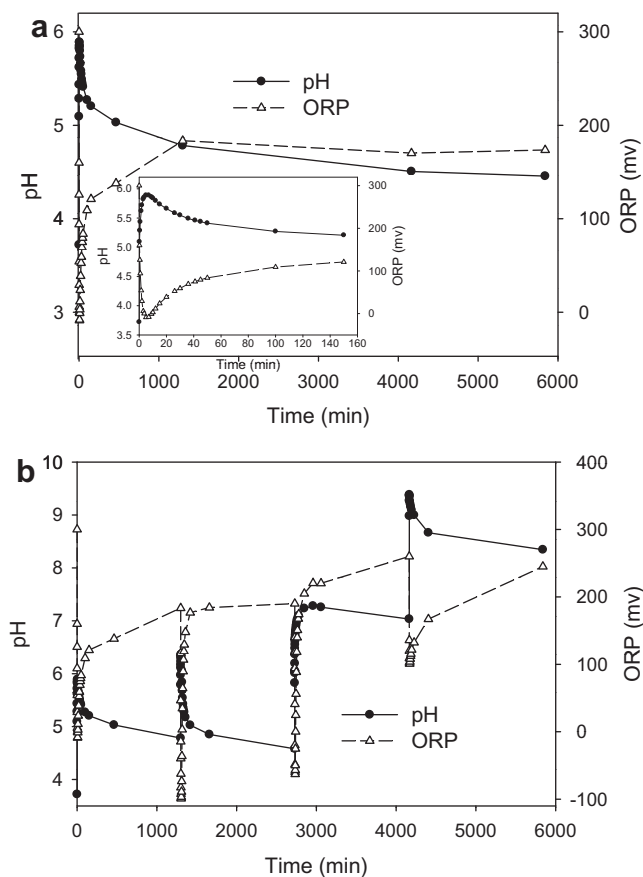
Fig. 6. Kinetics of pH and oxidation–reduction potential (ORP) changes in Lower Red Eyes water during abiotic neutralization/precipitation experiments. Results shown after addition of one aliquot of NaOH that yielded a final suspension of pH 4.38 (a). Inset in (a) details initial kinetics. Results shown for complete discontinuous neutralization where four aliquots of NaOH were added over four days and yielded a final suspension of pH 8.35 (b). Note that ORP values are relative to a +228 mV Zobel solution.

we did rinse these solids with distilled–deionized water before drying and digesting. Sulfate and other weakly adsorbed elements were likely removed to some unquantified extent by this water rinsing. Based on solid-phase Fe and S concentrations measured in ammonium oxalate and HCl digestions, the crystalline mineral fraction was highest for the precipitates formed at pH 4.38 and 4.40 (Table 3), consistent with higher estimated fractions of goethite for these samples (based on Fe EXAFS LC fitting; Table 2). For precipitates formed above pH 7, concentrations of Fe and S measured in the oxalate and HCl digestions were near equal, consistent with higher proportions of poorly crystalline minerals (i.e., schwertmannite and ferrihydrite). In contrast, S and Fe concentrations measured in the field sediments were much higher in the HCl digestions as compared to the oxalate digestions (Table 3). XRD peaks from field sediments (Figs. 3a and 4) could have been broadened by nanocrystalline phases (i.e., short-range ordered phases resistant to oxalate dissolution) of schwertmannite and goethite thereby confounding our operational distinction of crystalline versus poorly crystalline phases for certain samples.

The mineralogy of the abiotic precipitates formed from Lower Red Eyes water clearly differed from the natural

sediments collected from Lower Red Eyes (compare Fig. 4a with 7a), and clearly differed from the natural sediments collected from Fridays-2 (Table 2). The large fraction of ferrihydrite found in the abiotic precipitates formed at high pH is consistent with other studies (Bigham et al., 1996; Murad and Rojik, 2003). The formation of ferrihydrite over a more crystalline phase such as goethite or lepidocrocite could be promoted by dissolved species in the Lower Red Eyes water. For example, the presence of Si or Al favors the formation of ferrihydrite over lepidocrocite during oxidative hydrolysis of Fe(II) (Schwertmann and Thalmann, 1976; Taylor and Schwertmann, 1978). Both of these elements were present at high concentrations in the Lower Red Eyes water (Table 1), where Al was 1590 µM (Al/Fe(II) = 0.16) and Si was 423 µM (Si/Fe(II) = 0.04).

The incorporation of Al and Fe into the abiotic precipitates was confirmed by measuring the loss from solution of these elements from the supernatant of the neutralized suspensions (R-hand portions of Fig. 8). In the abiotic experiments, at final pH values of 4.38 and 4.40, Al (C_i = 1.6 mM) was removed to a greater relative extent ($C_{final\ pH}/C_i$ = 0.083–0.22; i.e., 91.7–88% removal) as compared to Fe (C_i = 8.9 mM; $C_{final\ pH}/C_i$ = 0.29–0.67). At fi-
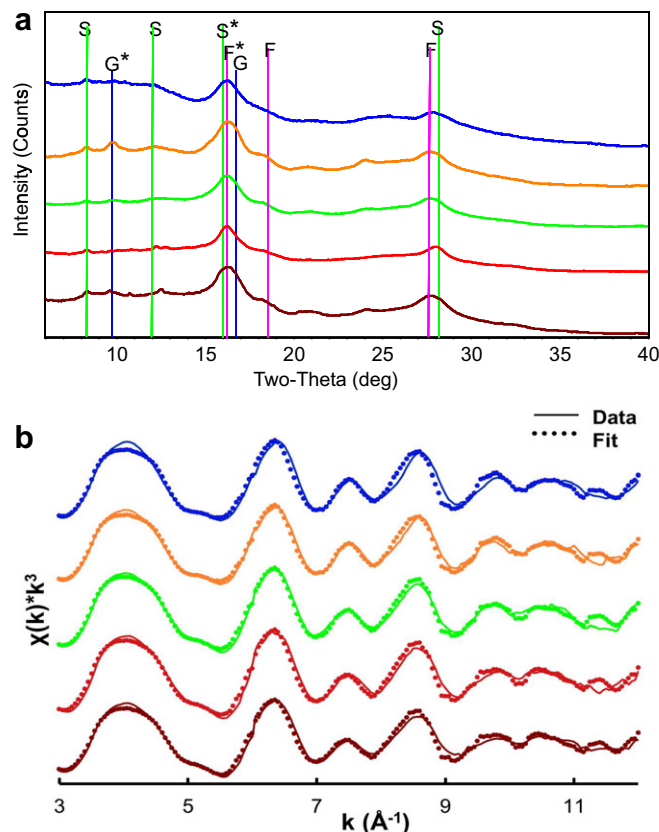
Fig. 7. X-ray diffraction patterns (a) and Fe K-edge EXAFS spectra (b) from solids formed in the lab from Lower Red Eyes water via abiotic neutralization/precipitation. Patterns are arranged top to bottom, respectively, for samples with lowest to highest final pH values and are in identical order in (a) and (b). Top pattern from pH 4.38 suspension, 2nd pattern from pH 4.40 suspension, 3rd pattern from pH 7.03 suspension, 4th pattern from pH 8.13 suspension, and bottom pattern from pH 8.35 suspension. In (a) F = ferrihydrite, G = goethite, S = schwertmannite, and * designates peak with greatest intensity in reference pattern. Details for fits of the Fe K-edge EXAFS spectra in (b) are provided in Table 2.

nal pH values >7, dissolved Fe and Al concentrations were always <50 μg/L.

We include dissolved metal concentrations as a function of pH on the iron mound in the L-hand portions of Fig. 8 to compare metal loss from solution in the field with the abiotic precipitates formed in the laboratory. In this unconventional plot, the dashed vertical line represents the emergent CMD spring, while points to the left represent sample sites further downstream of the CMD spring (where pH values continue to decline due to greater biological Fe(II) oxidation and Fe(III) hydrolysis) and points to the right represent laboratory samples with more NaOH addition. No metals other than Fe were removed across the Lower Red Eyes iron mound (L-hand portions of Fig. 8). Metal cations were not lost from surface waters in the field because of unfavorable electrostatic attraction to the iron mound minerals (i.e., schwertmannite). The pH of the surface waters decreased from ca. pH 4.0 to 2.5 across the iron mounds. The pH of zero point of charge (pH_{zpc}) of schwertmannite has been reported to be 7.2 (Johnson et al., 2005), thus metal cations would not be strongly attracted to the surface of schwertmannite at the low pH values found in the field. This result is consistent with other related field studies (Sidenko and Sherriff, 2005; Nagano et al., 2011).

Zinc, nickel and cobalt were the trace metals detected at the highest concentrations in the emergent AMD spring at Lower Red Eyes (Table 1). The removal of these metals from solution via NaOH addition was similar to the behavior of Fe and Al. At final pH values of 4.38–4.40, Ni was removed to a greater extent ($C_i = 233$ μM; $C_{final\ pH}/C_i = 0.33$–0.37) as compared to Zn ($C_i = 199$ μM; $C_{final\ pH}/C_i = 0.84$–0.98), and as compared to Co ($C_i = 70$ μM; $C_{final\ pH}/C_i = 0.95$–1.0). At final pH values >5, $C_{final\ pH}/C_i$ ratios were 0.042 ± 0.030 for Ni ($n = 7$), 0.015 ± 0.013 for Zn, and 0.10 ± 0.10 ($n = 7$) for Co. Greater removal of these metals at pH values >5 was confirmed based on corresponding increased solid-phase concentrations (Table 3). Based on oxalate and HCl digestions, the majority of these trace metals were associated with poorly crystalline minerals, especially for solids formed above pH 7.

4. DISCUSSION

The remediation of CMD focuses primarily on the removal of metals and acidity. Active CMD treatment refers to the continuous addition of chemicals and collection of metal precipitates. The most common active treatment processes are aeration and alkali addition to neutralize acidity
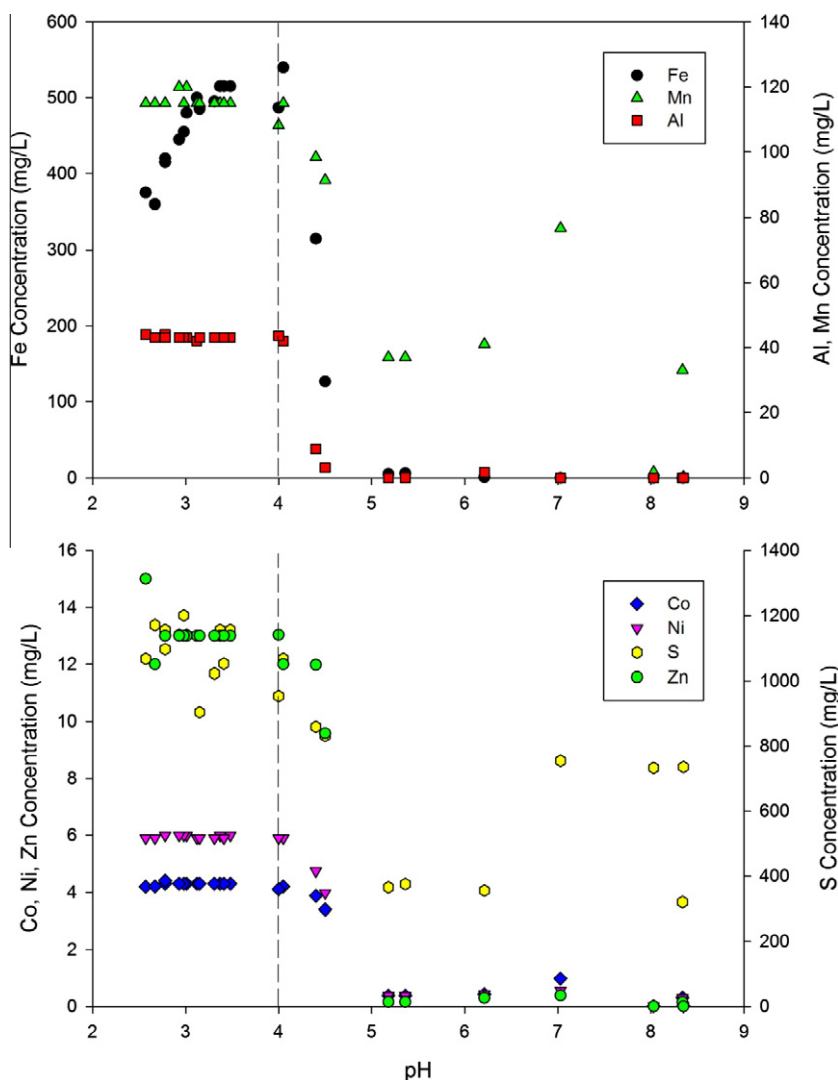
Fig. 8. Concentrations of dissolved elements in Lower Red Eyes water plotted as a function of pH. The dashed line indicates conditions at the emergent AMD spring. Left of the dashed line corresponds to field conditions downstream of the spring. Right of the dashed line corresponds to abiotic neutralization/precipitation in the laboratory. Note secondary axes for certain elements.

and promote rapid oxidation of Fe^{2+} and precipitation of Fe^{3+}, Al^{3+} and other metal contaminants. Depending on alkali dosing conditions, effective removal of Mn via oxidative hydrolysis of Mn^{2+} may or may not occur. Sodium hydroxide and calcium oxide are the most commonly used neutralizing agents for CMD active treatment. Alkali dosing is targeted to slightly exceed the total load (flow * concentration) of hot peroxide acidity of the influent CMD and results in abrupt geochemical changes. For example, it is not uncommon to see blue-green Fe(II)-rich and/or $Fe(OH)_2(s)$-containing water immediately downstream of the alkali dosing location. Even with settling ponds open to the atmosphere, the oxygen demand caused by high Fe(II) concentrations can allow reducing conditions to persist for some time. As aeration continues, the blue-green water eventually converts to an orange-red color indicative of Fe(III)-rich and/or $Fe(OH)_3(s)$-containing water. We describe these field observations because our laboratory neu-

tralization experiments essentially mimicked geochemical conditions encountered during CMD active treatment.

A number of studies have examined the stability of Fe precipitates formed in AMD and the corresponding controls on trace metals and metalloids. A portion of these studies began their experiments with minerals pre-formed in the field and/or via laboratory synthesis and monitored phase transformations and metal release/uptake as a function of time or as a function of solution chemistry (Bigham et al., 1996; Jönsson et al., 2005; Kumpulainen et al., 2008; Paikaray and Peiffer, 2010). At pH 2.5–4.0 goethite is often the sole transformation product of schwertmannite, while at pH >4.5–6.0 ferrihydrite and goethite are both produced (Bigham et al., 1996; Sánchez-España et al., 2011). Schwertmannite transformation to goethite is slow, often requiring hundreds of days, but conflicting results have been reported regarding the effect of pH. Two studies have reported that transformation to goethite was faster at high pH as com-

pared to low pH (Regenspurg et al., 2004; Jönsson et al., 2005; Schwertmann and Carlson, 2005), while one study reported that transformation was faster at low pH (Kumpulainen et al., 2008). These conflicting reports are likely caused by differing concentrations of constituents that can stabilize schwertmannite (e.g., Si, P, TOC – Jones et al., 2009; SO_4 – Knorr and Blodau, 2007) and/or Fe speciation that can control the importance of Fe(II)-induced conversion of schwertmannite (Burton et al., 2008).

Another group of studies more similar to our laboratory experiments involved using metal-rich solutions that abruptly became supersaturated due to aeration (Johnston et al., 2011) or neutralization (Lee et al., 2002; Sánchez-España et al., 2011) and then were monitored for phase transformations and release/uptake of metals and metalloids. Under these conditions trace metals can be removed from solution via (i) adsorption onto freshly formed mineral surface(s), (ii) co-precipitation into the mineral structure(s), and/or (iii) precipitation as "discrete" trace metal solid phases (e.g., $Me(OH)_x(s)$). The partitioning of adsorbed or co-precipitated trace metals can be subsequently affected by any phase transformation of the initial precipitate (e.g., schwertmannite) into secondary products (e.g., goethite). These studies have also focused on arsenic because it is a key contaminant of concern in the Iberian Pyrite Belt (Sánchez-España et al., 2011) and in Australian coastal lowland acid sulfate soils (Johnston et al., 2011). Arsenic, however, is not an important contaminant in Appalachian CMD. For example, in one survey of 156 CMD sources in Pennsylvania, the median As concentration was 0 μg/L (no detection limit reported; Watzlaf et al., 2002). In another survey of 99 CMD sources in the bituminous coal mining region of Pennsylvania (same as current study), the median As concentration was 2.0 μg/L (Cravotta, 2008).

Instead of arsenic, Fe, Al, Mn and acidity are the primary contaminants of concern in CMD. Active treatment using aeration and NaOH addition was clearly effective in removing Fe and Al (and Mn at highest pH values) from Lower Red Eyes water (Fig. 8). Based on reaction path modeling for Fe, schwertmannite would precipitate at pH >4.5 and ferrihydrite would precipitate at pH >6.2 if goethite precipitation was suppressed within the model (Electronic Annex, Fig. EA-6). If goethite precipitation was not suppressed, then it became thermodynamically stable throughout the entire pe-pH range over schwertmannite and ferrihydrite, indicating that all three Fe(III) minerals could form under these geochemical conditions. The simultaneous occurrence of schwertmannite, ferrihydrite, goethite and lepidocrocite (near pH 5.5) was observed in similar AMD titrations (Jönsson et al., 2006). Based on Fe EXAFS (Table 2), schwertmannite, goethite and ferrihydrite were all present in the abiotic precipitates, including those collected at final pH values >4.5. We speculate that both schwertmannite and ferrihydrite were the initial Fe phases to nucleate in these suspensions (Bigham et al., 1996; Schwertmann and Carlson, 2005) while goethite formed as a secondary product from schwertmannite (Regenspurg et al., 2004; Burton et al., 2008).

Based on reaction path modeling for Al, hydrobasaluminite ($Al_4(SO_4)(OH)_{10} \cdot 15H_2O$) would precipitate near pH 4.0 and was predicted to be the predominant solid Al phase throughout the entire pe-pH range of our experiments if $Al(OH)_3$ precipitation was suppressed in the model (Electronic Annex, Fig. EA-7). Inclusion of basaluminite instead of hydrobasaluminite yielded similar model predictions but we chose hydrobasaluminite because no dehydration to basaluminite would be expected to occur in these fresh, fully hydrated suspensions. If $Al(OH)_3$ precipitation was not suppressed, then it became predominant throughout the entire pe-pH range over hydrobasaluminite indicating that both hydrobasaluminite and $Al(OH)_3$ could form in our experiments. In Australian coastal lowland acid sulfate soils, a combination of basaluminite and amorphous $Al(OH)_3$ were found to control dissolved Al^{3+} concentrations between pH 3–7 (Jones et al., 2011). In Pennsylvanian coal mine drainage, a combination of amorphous $Al(OH)_3$ and a poorly crystalline aluminum hydroxysulfate were found to control dissolved Al^{3+} concentrations above pH 5 (Pu et al., 2010). In our experiments, Al was detected in the abiotic precipitates by SEM-EDS but we were unable to resolve whether the Al signal originated from morphologically unique particles (i.e., as Al solids vs. co-precipitated with Fe solids). However, because Al solids were predicted to form at pH values lower than when Fe solids were first predicted to form, Al was likely removed both as hydrobasaluminite (especially at low pH), amorphous $Al(OH)_3$, and/or as a co-precipitate into schwertmannite or ferrihydrite. It was unclear whether jurbanite ($Al(OH)SO_4$) formed in our neutralization experiments, however, suppression of jurbanite substantially increased the accuracy of our reaction path modeling. In contrast to field sediments collected from Lower Red Eyes, Al concentrations were two to three orders of magnitude higher in the abiotic precipitates (Table 3).

Reaction path modeling for Zn, Ni and Co showed that these trace metals would not be removed from solution as their corresponding $Me(OH)_2(s)$ phases at the pH values that we observed for their removal. Therefore, adsorption to or co-precipitation in schwertmannite, ferrihydrite, and hydrobasaluminite were the predominant trace metal removal mechanisms in our experiments. This interpretation is supported by the results from the oxalate and HCl digestions, where the majority of trace metals were associated with poorly crystalline minerals (Table 3). Similar results have been reported by Lee et al. (2002) using AMD generated from the mining of massive sulfide ore deposits in eastern Tennessee. Using one fully oxidized, Fe-rich AMD sample (pH 2, 12 mM Fe, 21 mM SO_4^{2-}) that was similar to Lower Red Eyes CMD, they found that Fe was removed from solution at pH >3, Al was removed at pH >5, and Mn was removed at pH >8. The removal of Cd, Co, Cu, Pb and Zn occurred fairly sharply over different pH ranges for each metal but complete removal of all metals did not occur until pH >8. In the current study, we found that removal of Fe, Al, Co, Ni and Zn all occurred fairly sharply and somewhat simultaneously at pH >5 (Fig. 8). As noted above, removal of metal cations (except Fe) did not occur in the field be-

cause of limited sorption at pH <4 (Sidenko and Sherriff, 2005; Nagano et al., 2011).

Biological low-pH Fe(II) oxidation could be a very useful pre-treatment step in the remediation of AMD. Fe and acidity loads could be decreased before conventional active or passive treatment processes, thereby decreasing the size and cost of these units. Removal of any iron and acidity before passive treatment limestone beds will improve performance by decreasing limestone armoring, decreasing hydraulic clogging by Fe precipitates, and decreasing the acidity load. Removal of any iron and acidity before active treatment via neutralization will reduce costs by decreasing alkali chemical requirements and decreasing Fe sludge production. Furthermore, in portions of the Appalachian coal mining region where As or other anionic contaminants such as Se are present at only exceptional low concentrations, the Fe(III) precipitates should be essentially free of trace metal and metalloid contaminants. The mineral composition of iron mounds produced by low-pH Fe(II) oxidation of Appalachian CMD appeared to be similar at all of the field sites we studied both spatially across any one site and comparatively between any two sites. Based on metal oxide contents measured after lithium metaborate fusion (Electronic Annex, Table EA-1), Fe_2O_3 contents of 50–67% approached values of Fe ore bodies (Hedin, 2003). Because of their high Fe content, mineralogical purity and absence of trace contaminants, these iron mound sediments could prove to be of considerable economic value (Janneck et al., 2010).

Iron mounds and low-pH Fe(II) oxidation are often underappreciated by watershed professionals responsible for designing AMD remediation systems. In many cases significant amounts of Fe and associated acidity are naturally and passively removed by these mounds. Assuming that we can better understand the biogeochemistry of this process, we should be able to exploit and engineer it for even greater treatment. Water discharged from these mounds would still have to be neutralized to remove acidity and trace metals but the iron and acidity loads going into downstream systems could be dramatically reduced. If the iron mound sediments were periodically collected and sold for some industrial purpose (e.g., anion adsorbents, pigments, ceramics) then any profit could be invested back into additional AMD treatment systems. Future research will hopefully develop the economic and environmental sustainability of these efforts.

ACKNOWLEDGMENTS

APPENDIX A. SUPPLEMENTARY DATA

Supplementary data associated with this article can be found, in the online version, at doi:10.1016/j.gca.2011.10.015.

REFERENCES

Acero P., Ayora C., Torrentó C. and Nieto J.-M. (2006) The behavior of trace elements during schwertmannite precipitation and subsequent transformation into goethite and jarosite. *Geochim. Cosmochim. Acta* **70**, 4130–4139.

Bigham J. M., Schwertmann U., Carlson L. and Murad E. (1990) A poorly crystallized oxyhydroxysulfate of iron formed by bacterial oxidation of Fe(II) in acid mine waters. *Geochim. Cosmochim. Acta* **54**, 2743–2758.

Bigham J. M., Schwertmann U., Traina S. J., Winland R. L. and Wolf M. (1996) Schwertmannite and the chemical modeling of iron in acid sulfate waters. *Geochim. Cosmochim. Acta* **60**, 2111–2121.

Borch T., Masue Y., Kukkadapu R. K. and Fendorf S. (2006) Phosphate imposed limitations on biological reduction and alteration of ferrihydrite. *Environ. Sci. Technol.* **41**, 166–172.

Brown J. F., Jones D. S., Mills D. B., Macalady J. L. and Burgos W. D. (2010) Application of a depositional *facies* model to an acid mine drainage site. *Appl. Environ. Microbiol.*. AEM.01550–01510.

Burton E. D., Bush R. T., Sullivan L. A. and Mitchell D. R. G. (2008) Schwertmannite transformation to goethite via the Fe(II) pathway: reaction rates and implications for iron-sulfide formation. *Geochim. Cosmochim. Acta* **72**, 4551–4564.

Collins R. N., Jones A. M. and Waite T. D. (2010) Schwertmannite stability in acidified coastal environments. *Geochim. Cosmochim. Acta* **74**, 482–496.

Cravotta C. A. (2008) Dissolved metals and associated constituents in abandoned coal-mine discharges, Pennsylvania, USA. Part 1: constituent quantities and correlations. *Appl. Geochem.* **23**, 166–202.

DeSa T., Brown J. and Burgos W. (2010) Laboratory and field-scale evaluation of low-pH Fe(II) oxidation at Hughes Borehole, Portage, Pennsylvania. *Mine Water Environ.* **29**, 239–247.

Fouke B. W., Farmer J. D., Des Marais D. J., Pratt L., Sturchio N. C., Burns P. C. and Discipulo M. K. (2000) Depositional *facies* and aqueous-solid geochemistry of travertine-depositing hot springs (Angel Terrace, Mammoth Hot Springs, Yellowstone National Park, USA). *J. Sediment. Res.* **70**, 565–585.

Hansel C. M., Benner S. G., Neiss J., Dohnalkova A., Kukkadapu R. K. and Fendorf S. (2003) Secondary mineralization pathways induced by dissimilatory iron reduction of ferrihydrite under advective flow. *Geochim. Cosmochim. Acta* **67**, 2977–2992.

Hedin R. S., Watzlaf G. R. and Nairn R. W. (1994) Passive treatment of acid mine drainage with limestone. *J. Environ. Qual.* **23**, 1338–1345.

Hedin R. S. (2003) Recovery of marketable iron oxide from mine drainage in the USA. *Land Contam. Reclaminat.* **11**, 93–97.

Herlihy A., Kaufmann P., Mitch M. and Brown D. (1990) Regional estimates of acid mine drainage impact on streams

in the mid-atlantic and Southeastern United States. *Water Air Soil Pollut.* **50**, 91–107.

Jacquat O., Voegelin A. and Kretzschmar R. (2009) Soil properties controlling Zn speciation and fractionation in contaminated soils. *Geochim. Cosmochim. Acta* **73**, 5256–5272.

Janneck E., Arnold I., Koch T., Meyer J., Burghardt D. and Ehinger S. (2010) Microbial synthesis of schwertmannite from lignite mine water and its utilization for removal of arsenic from mine waters and for production of iron pigments. Mine Water and Innovative Thinking, Sydney, NS.

Johnson D. B., Okibe N. and Hallberg K. B. (2005) Differentiation and identification of iron-oxidizing acidophilic bacteria using cultivation techniques and amplified ribosomal DNA restriction enzyme analysis. *J. Microbiol. Methods* **60**, 299–313.

Johnston S. G., Keene A. F., Burton E. D., Bush R. T. and Sullivan L. A. (2011) Iron and arsenic cycling in intertidal surface sediments during wetland remediation. *Environ. Sci. Technol.* **45**, 2179–2185.

Jones A. M., Collins R. N., Rose J. and Waite T. D. (2009) The effect of silica and natural organic matter on the Fe(II)-catalysed transformation and reactivity of Fe(III) minerals. *Geochim. Cosmochim. Acta* **73**, 4409–4422.

Jones A. M., Collins R. N. and Waite T. D. (2011) Mineral species control of aluminum solubility in sulfate-rich acidic waters. *Geochim. Cosmochim. Acta* **75**, 965–977.

Jönsson J., Persson P., Sjöberg S. and Lövgren L. (2005) Schwertmannite precipitated from acid mine drainage: phase transformation, sulphate release and surface properties. *Appl. Geochem.* **20**, 179–191.

Jönsson J., Jönsson J. and Lövgren L. (2006) Precipitation of secondary Fe(III) minerals from acid mine drainage. *Appl. Geochem.* **21**, 437–445.

Kirby C. S. and Cravotta Iii C. A. (2005) Net alkalinity and net acidity 1: theoretical considerations. *Appl. Geochem.* **20**, 1920–1940.

Knorr K.-H. and Blodau C. (2007) Controls on schwertmannite transformation rates and products. *Appl. Geochem.* **22**, 2006–2015.

Kumpulainen S., Carlson L. and Räisänen M.-L. (2007) Seasonal variations of ochreous precipitates in mine effluents in Finland. *Appl. Geochem.* **22**, 760–777.

Kumpulainen S., Raisanen M.-L., Von Der Kammer F. and Hofmann T. (2008) Ageing of synthetic and natural schwertmannites at pH 2–8. *Clay Mineral.* **43**, 437–448.

Lane D. J., Harrison, Jr., A. P., Stahl D., Pace B., Giovannoni S. J., Olsen G. J. and Pace N. R. (1992) Evolutionary relationships among sulfur- and iron-oxidizing eubacteria. *J. Bacteriol.* **174**, 269–278.

Lee G., Bigham J. M. and Faure G. (2002) Removal of trace metals by coprecipitation with Fe, Al and Mn from natural waters contaminated with acid mine drainage in the Ducktown Mining District, Tennessee. *Appl. Geochem.* **17**, 569–581.

Lucas M. A. (2008) The comparison of two acid mine drainage sites in central Pennsylvania: field site characterizations and batch reactor experiments. M. S. Thesis, The Pennsylvania State Univ., University Park, PA, USA, pp. 172.

Moberly J., Borch T., Sani R., Spycher N., Şengör S., Ginn T. and Peyton B. (2009) Heavy metal–mineral associations in Coeur d'Alene river sediments: a synchrotron-based analysis. *Water Air Soil Pollut.* **201**, 195–208.

Murad E. and Rojik P. (2003) Iron-rich precipitates in a mine drainage environment: influence of pH on mineralogy. *Am. Mineral.* **88**, 1915–1918.

Nagano T., Yanase N., Hanzawa Y., Takada M., Mitamura H., Sato T. and Naganawa H. (2011) Evaluation of the affinity of some toxic elements to schwertmannite in natural streams contaminated with acid mine drainage. *Water Air Soil Pollut.* **216**, 153–166.

Paikaray S. and Peiffer S. (2010) Dissolution kinetics of sulfate from schwertmannite under variable pH conditions. *Mine Water Environ.* **29**, 263–269.

Pennsylvania Department of Environmental Protection (PA DEP). (2006) The Development of a Mine Drainage Restoration Plan for Bennett Branch, Sinnemahoning Creek: Clearfield, Elk, and Cameron Counties, Pennsylvania.

Peretyazhko T., Zachara J. M., Boily J. F., Xia Y., Gassman P. L., Arey B. W. and Burgos W. D. (2009) Mineralogical transformations controlling acid mine drainage chemistry. *Chem. Geol.* **262**, 169–178.

Pu X., Vazquez O., Monnell J. D. and Neufeld R. D. (2010) Speciation of aluminum precipitates from acid rock discharges in Central Pennsylvania. *Environ. Eng. Sci.* **27**, 169–180.

Regenspurg S., Brand A. and Peiffer S. (2004) Formation and stability of schwertmannite in acidic mining lakes. *Geochim. Cosmochim. Acta* **68**, 1185–1197.

Sánchez-España J., Yusta I. and Diez-Ercilla M. (2011) Schwertmannite and hydrobasaluminite: a re-evaluation of their solubility and control on the iron and aluminium concentration in acidic pit lakes. *Appl. Geochem.* **26**, 1752–1774.

Schwertmann U. and Thalmann H. (1976) The influence of [Fe(II)], [Si], and pH on the formation of lepidocrocite and ferrihydrite during oxidation of aqueous FeCl$_2$ solutions. *Clay Mineral.* **11**, 189–200.

Schwertmann U. and Carlson L. (2005) The pH-dependent transformation of schwertmannite to goethite at 25 °C. *Clay Mineral.* **40**, 63–66.

Sidenko N. V. and Sherriff B. L. (2005) The attenuation of Ni, Zn and Cu by secondary Fe phases of different crystallinity from surface and ground water of two sulfide mine tailings in Manitoba, Canada. *Appl. Geochem.* **20**, 1180–1194.

Senko J. M., Wanjugi P., Lucas M., Bruns M. A. and Burgos W. D. (2008) Characterization of Fe(II) oxidizing bacterial activities and communities at two acidic Appalachian coalmine drainage-impacted sites. *ISME J.* **2**, 1134–1145.

Taylor R. M. and Schwertmann U. (1978) The influence of aluminum on iron oxides: Part 1. The influence of Al on Fe oxide formation from the Fe(II) system. *Clays Clay Miner.* **26**, 373–383.

United States Geological Survey (USGS). (2008) Coal mine drainage projects in Pennsylvania. US Geological Survey. <http://pa.water.usgs.gov/projects/energy/amd/> (accessed May 2, 2011).

Watzlaf G. R., Schroeder K. T., Kleinmann R. L. P., Kairies C. L. and Nairn R. W. (2002) *The Passive Treatment of Coal Mine Drainage*. American Society of Mining and Reclamation, Lexington, Kentucky.

Webb S. M. (2005) SIXpack: a graphical user interface for XAS analysis using IFEFFIT. *Phys. Scr.* **2005**, 1011.

Zhang G., Dong H., Kim J. and Eberl D. D. (2007) Microbial reduction of structural Fe^{3+} in nontronite by a thermophilic bacterium and its role in promoting the smectite to illite reaction. *Am. Mineral.* **92**, 1411–1419.

Associate editor: Donald L. Sparks